DESIGN AND EXPERIMENTAL STUDY OF A CONTROL SYSTEM FOR SYNCHRONIZED CORN SEEDING AND HOLE FERTILIZATION
/
玉米播种和穴播施肥同步控制系统的设计与试验研究

Ziyu WANG[1)], Hongchao WANG[2)], Chunying LIANG*[2)], Naichen ZHAO[2)]
[1)] College of Information and Electrical Engineering, Heilongjiang Bayi Agricultural University, Daqing 163319, China
[2)] College of Engineering, Heilongjiang Bayi Agricultural University, Daqing/China
Tel: 13836961615; E-mail: liangchunying@byau.edu.cn
DOI: https://doi.org/10.35633/inmateh-75-91

Keywords: *corn, hole fertilization, control system, experiment.*

ABSTRACT
To solve the problems of slow system response speed and poor uniformity of seeding and fertilizer application, this paper designs a control system for synchronized corn seeding and precision hole fertilization. A sliding mode control method with integral variable structure and disturbance observer composite (ISMDO-SMC) is proposed. Furthermore, a three-factor, five-level quadratic orthogonal rotation combination experiment was conducted to develop a mathematical model for parameter optimization using a multi-objective variable optimization method. Simulation results from four algorithms were compared, revealing a regulation time of 0.42 seconds, a recovery time to steady state of 0.13 seconds, and a descending rotational speed of 2.5 r/min, which demonstrates the strongest dynamic response and stability. Moreover, the optimal parameter combination was determined to be the forward speed of 2.8 km/h, the fertilizer discharge shaft speed of 42 r/min, and the fertilizer discharger opening of 5.5 mm, resulting in the fertilizer application error of 1.7 g and the seed-fertilizer spacing error of 2.2 mm. The results of this study provide a theoretical basis for achieving efficient and stable seeding and fertilization operations.

摘要
为了解决系统响应速度慢和播种施肥均匀性差的问题，本文设计了一种同步玉米播种与穴施肥的控制系统。提出了一种基于积分变量结构和扰动观测器复合的滑模控制方法。此外，采用三因素五水平的二次正交旋转组合实验，通过多目标变量优化方法建立了参数优化的数学模型。通过比较四种算法的仿真结果，得出该系统的调节时间为 0.42 秒，恢复稳态时间为 0.13 秒，下降转速为 2.5 r/min，表明其具有最强的动态响应和稳定性。进一步，优化的参数组合为前进速度 2.8 km/h，施肥轴转速 42 r/min，施肥器开度 5.5 mm，在此条件下，施肥误差为 1.7 g，种肥间距误差为 2.2 mm。该研究结果为实现高效稳定的播种施肥作业提供了理论依据。

INTRODUCTION
Corn is an important food and income crop that holds a significant position in global agriculture. In corn production, fertilizer application plays a crucial role in ensuring both high yield and high quality *(Yu et al., 2021)*. Traditional fertilizer application methods typically involve manual application or the use of fertilizer spreaders to distribute fertilizer across the ground surface *(Vieira-Megda et al., 2015)*. However, these methods increase production costs and result in low fertilizer utilization, preventing the achievement of spatially differentiated fertility replenishment *(Zhang et al., 2012)*. Irrational fertilizer application not only leads to environmental pollution but also negatively affects crop yield and quality *(Qi et al., 2024)*. Control systems that synchronize corn seeding with precision hole fertilization are an integral component of sustainable precision agriculture systems. These systems enhance fertilizer use and yield while reducing application rates and mitigating the environmental pressures caused by over-fertilization.

In recent years, variable fertilization techniques have gained increasing attention in several countries *(Cheng et al., 2022)*. Japan's Iseki Agricultural Machinery Co., Ltd. has developed a series of self-propelled variable spray fertilizer applicators for paddy fields. These machines are equipped with a variable fertilizer application system that collects real-time information on soil nutrients and crop characteristics through various sensors. The amount of fertilizer applied is adjusted by the controller to meet the specific requirements for crop growth *(Shi et al., 2019; Yu et al., 2019; Chen et al., 2019)*.

[1] *Ziyu Wang, master degree*; *Hongchao Wang, Ph.D.*; *Chunying Liang, Prof. Ph.D.*; *Naichen Zhao, Ph.D.*

To achieve refined operations, some researchers have extensively explored aspects such as fertilizer prescription decisions and variable control algorithms. Tola developed a fertilizer control system based on real-time fertilizer discharge sensors, which has reduced fertilizer application errors (*Tola et al., 2008*). Bu proposed an optimization model for the fertilization control sequence based on a differential evolutionary algorithm, enabling online regulation of fertilizer application and improving fertilization performance (*Bu et al., 2022*). The control system is the core of variable fertilizer application technology and plays a decisive role in the effectiveness of fertilizer application. A significant number of scholars have widely adopted the external grooved wheel fertilizer application method for variable fertilizer application, with fertilizer volume adjustment achieved by altering the rotational speed of the fertilizer discharge shaft. Sugirbay investigated the effect of groove wheel parameters on the stability of high-speed fertilizer discharging in external groove wheel fertilizer dischargers. They designed 25 groove wheel configurations and conducted bench tests to identify the optimal parameters and speed range (*Sugirbay et al., 2020*). Alameen developed a variable-speed granular fertilizer application control system that uses cylinders to regulate the openings of all fertilizer dischargers. This system was able to accurately control the rate of granular fertilizer application, with an overall system error of less than 2.6% *(Alameen, Al-Gaadi, & Tola, 2019)*. In summary, numerous scholars have conducted in-depth research on fertilizer application devices and control systems *(Pramod et al., 2023; Wang et al., 2023)*. However, issues such as slow system response time and poor uniformity in seeding and fertilizer application during corn seeding and hole fertilization still require further investigation. Addressing these challenges is crucial for improving the overall performance and adaptability of fertilizer application devices, and for providing stronger technical support for the realization of precision agriculture.

The main objective of this study is to design a control system for synchronizing corn seeding and variable hole fertilization. An integral sliding mode variable structure controller was designed, and a novel convergence rate was introduced to significantly improve both the steady-state and dynamic performance of the control system. Additionally, the system incorporates an extended state observer to monitor perturbations caused by changes in motor parameters and load torque. The observed perturbation values are then fed into the sliding mode controller as feed-forward compensation, enhancing the system's ability to resist interference. Furthermore, the performance of the control system for synchronized variable hole fertilization during corn seeding was validated through a bench experiment.

MATERIALS AND METHODS

Machine Structure and Working Principle

The experimental bench primarily consists of a conveyor platform, a box, a corn hole application device, a seed discharger, a control system, and a photoelectric detection device, as shown in figure 1. The fertilizer and seed boxes are filled with fertilizer and seeds, respectively, and the conveyor belt moves at a constant speed once the power is turned on, simulating the relative motion between the locomotive and the field. Upon activating the system, the fertilizer discharge motor is first controlled to rotate, ensuring the preparation of fertilizer for the first hole application. The photoelectric sensor probe installed at the outlet of the seed discharger detects the seed, transmits the signal to the microcontroller, and controls the rotation of the fertilizer discharge tube stopper to a set angle, aligning the fertilizer discharge opening with the circular notch on the stopper to synchronize seeding and fertilizer application.

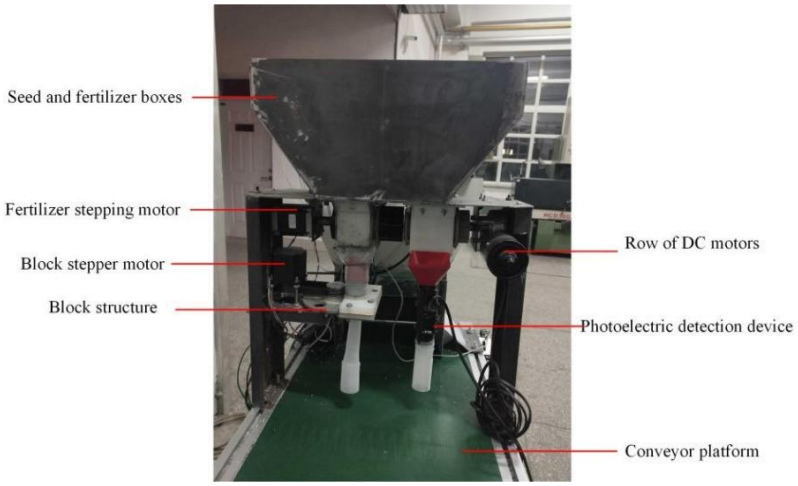

Fig. 1 - Experimental bench for synchronized corn seeding and precision hole fertilization

A disc stopper was designed to control the intermittency of the fertilizer discharge at the fertilizer discharge opening, using a non-corrosive plastic material. The stopper has three holes that are 120° apart from the center of the circle, the same size as the fertilizer pipe. The position of the baffle round hole coincides with the position of the mouth of the fertilizer discharge tube, allowing the fertilizer to fall through the round hole. The stopper is closed when the stopper round hole is turned 60°. The fertilizer builds up above the stopper, providing enough fertilizer for the next time the stopper switch is turned on. During this time the fertilizer discharged from the discharger is stored in the tube. The physical drawing of the stopper structure of the fertilizer discharge port is shown in figure 2.

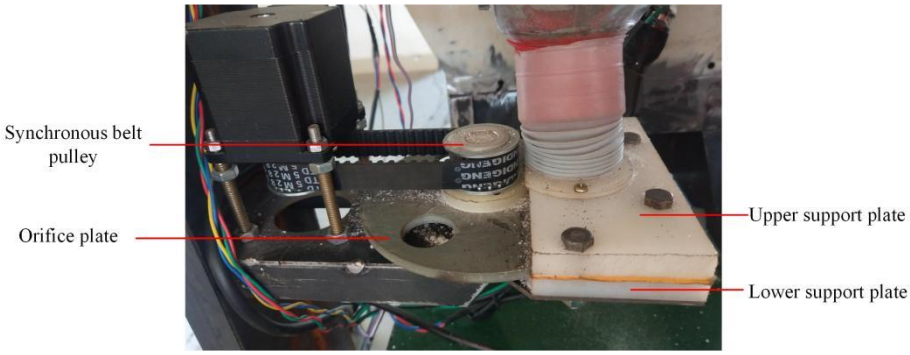

Fig. 2 - Physical drawing of the stopper structure of the fertilizer discharge port

Control System Design for Synchronization of Corn Seeding and Variable Hole Application of Fertilizer

The control system is an important part of the whole experimental bench, which is mainly composed of a data acquisition module, microcontroller control module, human-machine interface module, and actuator module, as shown in Fig. 3. The control system controls the fertilizer discharger by changing the motor speed for precise fertilizer discharge. The microcontroller chosen is the more commonly used STC15F2K60S2, which is simple to program, has a stable system, and lower cost. The single clock machine cycle of the microcontroller, the internal integration of high-precision R/C clock, and the highly reliable reset circuit make it a good option. The overall circuit diagram of the control system is shown in figure 4.

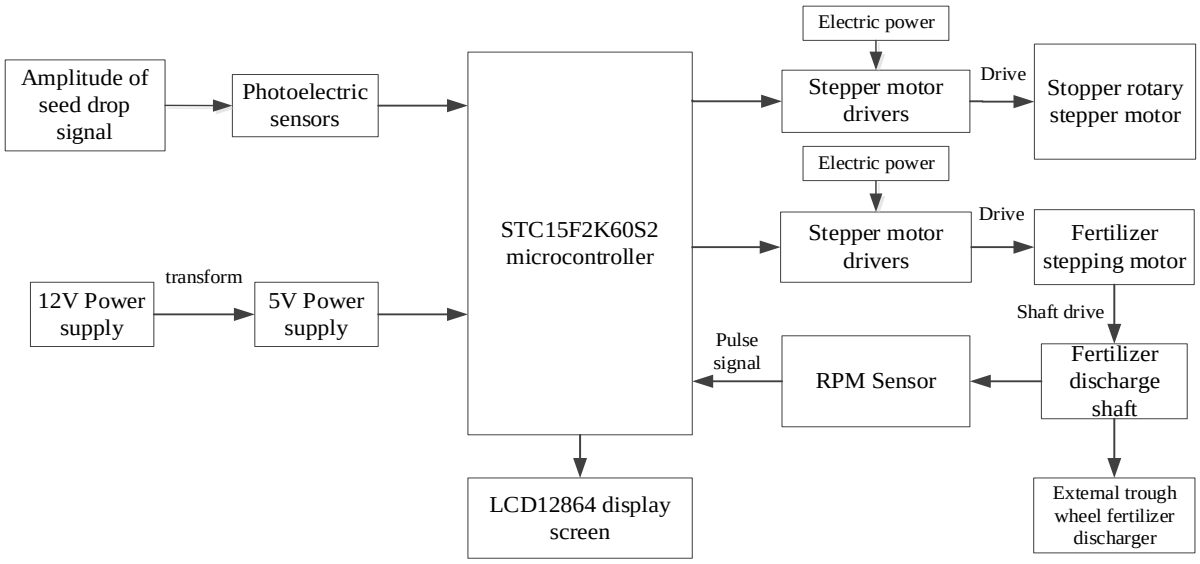

Fig. 3 - Hardware block diagram of the control system

After system initialization, the control system operates as in the flowchart is shown in figure 5. Initially, the motor controls the fertilizer spreader to rotate the corresponding number of slots, completing one fertilization cycle and waiting for the first seed to drop. Starting from the second fertilization cycle, when the photoelectric sensor detects a seed drop, it is necessary to determine whether the time interval since the previous drop is shorter than a predefined threshold. If the interval is shorter, it indicates a repeat drop, and the system returns to the waiting state.

Otherwise, it is considered a normal sowing cycle, and the corresponding pulse is immediately sent. The control flaps open and close at the corresponding angles to allow the prepared fertilizer to fall into the soil. After a delay, the flaps are closed at the specified angle, completing one cycle of hole fertilization, which repeats continuously. When no seed drop is detected, a missed sowing check is performed. If a missed sowing is detected, all interrupts are disabled, the fault code is displayed, and the system waits for a reset. Otherwise, it returns to continue waiting for the next seed drop.

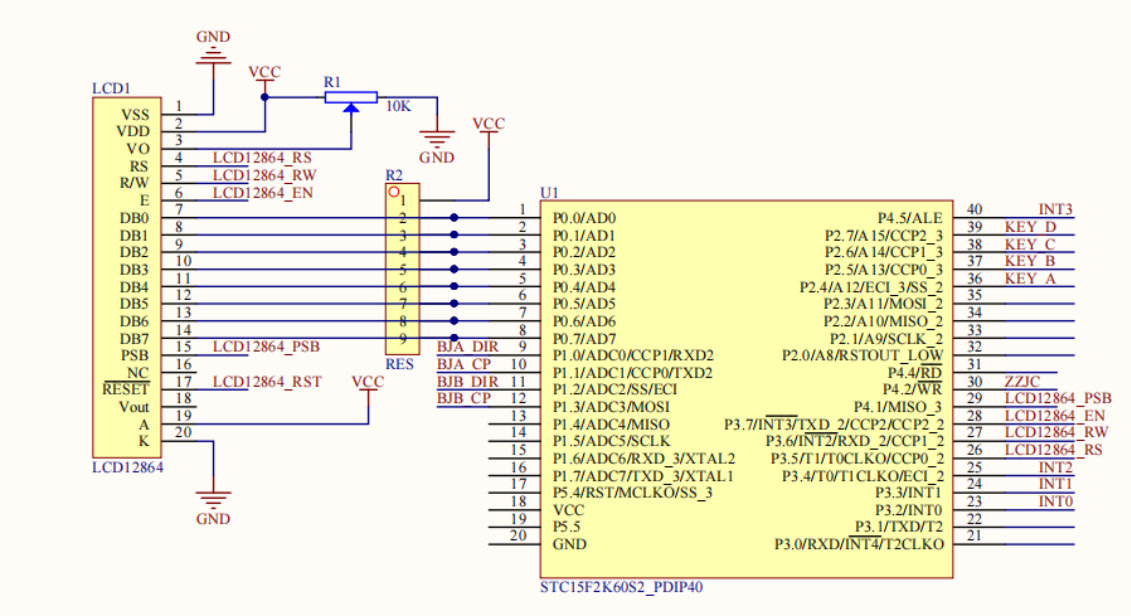

Fig. 4 - Overall circuit diagram of the control system

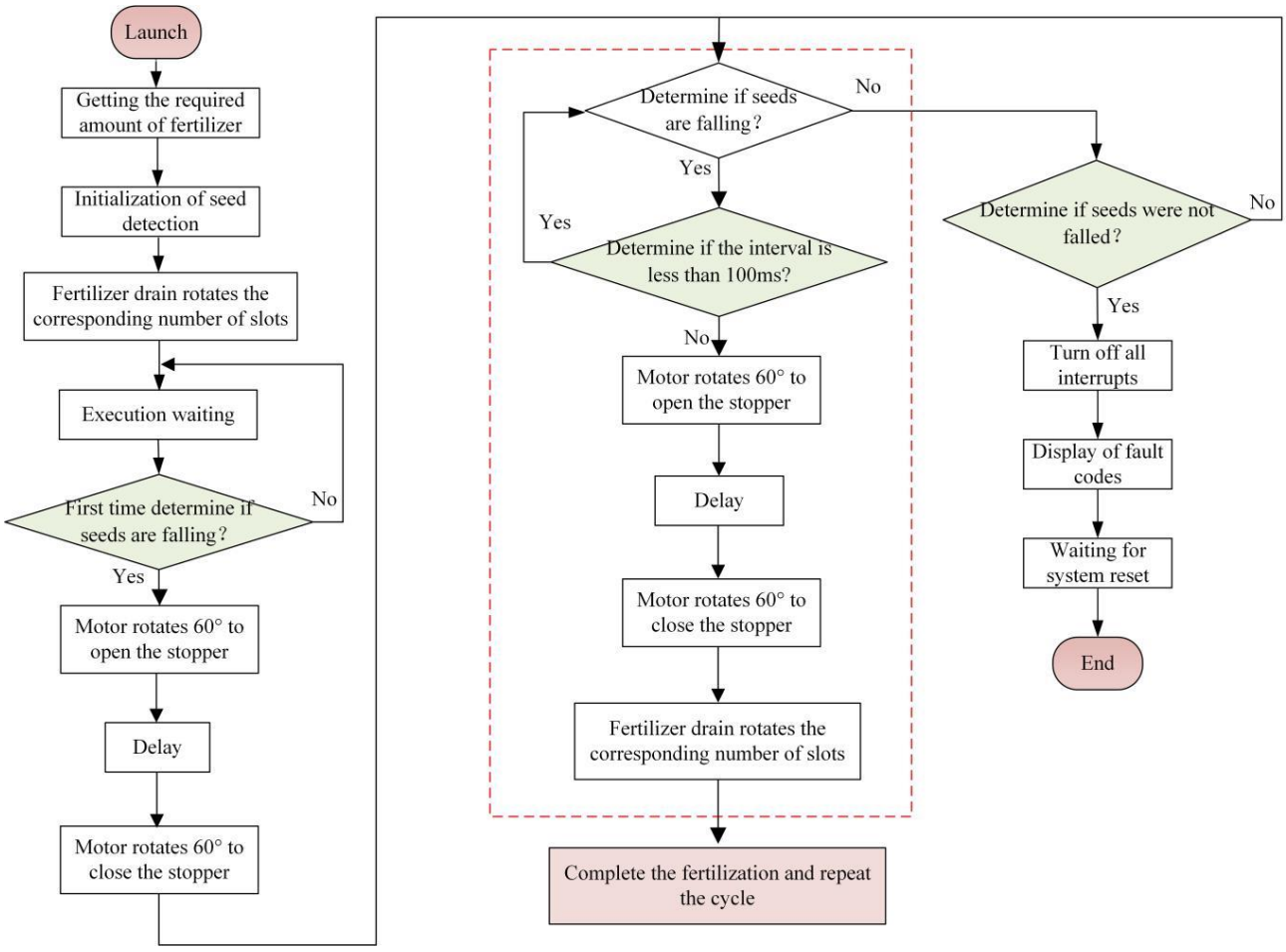

Fig. 5 - Control system flowchart

System Control Strategy

Mathematical Modeling of The Motor

Under the assumption of neglecting motor parameter variations and external disturbances, the mathematical model of the motor can be established, and the voltage equation is given by Equation (1).

$$\begin{cases} u_d = Ri_d + L_d \dfrac{\mathrm{d}i_d}{\mathrm{d}t} - p\omega_m L_q i_q \\ u_q = Ri_q + L_q \dfrac{\mathrm{d}i_q}{\mathrm{d}t} + p\omega_m L_d i_d + p\omega_m \psi_f \end{cases} \quad (1)$$

where:

u_d, i_d, L_d represent the voltage, current, and inductance on the d-axis, respectively;

u_q, i_q, L_q represent the voltage, current, and inductance on the q-axis, respectively;

R is the stator winding resistance; ω_m is the motor output speed; ψ_f is the magnetic chain;

p is the number of pole pairs.

Additionally, since the permanent magnet synchronous motor has $L_d = L_q$, the torque equation is given by equation (2), where T_e is the target torque.

$$T_e = \frac{3}{2} p \psi_f i_q \quad (2)$$

The equations of motion for the motor are given in Equation (3).

$$\frac{\mathrm{d}\omega_m}{\mathrm{d}t} = \frac{3p\psi_f}{2J} i_q - \frac{T_L}{J} - \frac{B}{J}\omega_m \quad (3)$$

where: B is the coefficient of viscous friction; J is the rotational inertia; T_L is the load torque.

Equation (4) is derived by considering the variation in system parameters and torque.

$$\frac{\mathrm{d}\omega_m}{\mathrm{d}t} = \left(\frac{3p\psi_f}{2J} + \Delta\alpha_1\right) i_q - \left(\frac{T_L}{J} + \Delta\alpha_2\right) - \left(\frac{B}{J} + \Delta\alpha_3\right)\omega_m = \frac{3p\psi_f}{2J} i_q - \frac{B}{J}\omega_m + \beta \quad (4)$$

$$\beta = \frac{3p\psi_f}{2J}\Delta\alpha_1 i_q - \Delta\alpha_2 - \frac{B}{J}\Delta\alpha_3\omega_m - \frac{T_L}{J} \quad (5)$$

where: $\Delta\alpha_1$, $\Delta\alpha_2$, $\Delta\alpha_3$ denote the values of parameter changes of the motor; β denotes the value of perturbation brought by the load torque and parameters.

Design Of Sliding Mode Controller

The motor state variable is given by Equation (6).

$$\begin{cases} x_1 = \omega_{ref} - \omega_m \\ \dot{x}_2 = \dot{x}_1 \end{cases} \quad (6)$$

where ω_{ref} is the target speed; The derivation of Equation (6) leads to Equation (7).

$$\begin{cases} \dot{x}_1 = -\left(\dfrac{3p\psi_f}{2J} i_q - \dfrac{B}{J}\omega_m + \beta\right) \\ \dot{x}_2 = -\left(\dfrac{3p\psi_f}{2J}\dot{i}_q - \dfrac{B}{J}\dot{\omega}_m + \dot{\beta}\right) \end{cases} \quad (7)$$

The system sliding mode surface function is defined by Equation (8).

$$s = cx_1 + x_2 \quad (8)$$

Substituting Equation (6) into Equation (8) yields the following:

$$\dot{s} = c\dot{x}_1 - \frac{3p\psi_f}{2J}\dot{i}_q + \frac{B}{J}\dot{\omega}_m - \dot{\beta} \tag{9}$$

In the actual motor control, the sliding mode control method suffers from high-frequency jitter. Therefore, it is necessary to select a suitable exponential convergence rate that can effectively attenuate the sliding mode jitter. To improve the system's performance, a novel, improved convergence rate will be introduced, as shown in Equation (10).

$$\begin{cases} \dot{s} = -\varepsilon|x_1|\mathrm{sgn}(s) - ks \\ \lim\limits_{t\to\infty} = |x_1| \end{cases} \tag{10}$$

where ε>0, k>0; -$\varepsilon|x_1|\mathrm{sgn}(s)$ is the isochronous convergence term; ks is the exponential convergence term.

As the error increases, the isochronous convergence term drives the system state variable toward the sliding mode surface, while the exponential convergence term reduces the system state variable to zero.

By combining Equations (9) and (10), the output equation of the controller is given by:

$$i_q^* = \frac{2J}{3p\psi_f}\int c\dot{x}_1 + \frac{B}{J}\dot{\omega}_m + \varepsilon|x_1|\mathrm{sgn}(s) + ks - \dot{\beta}\,\mathrm{d}t \tag{11}$$

The Lyapunov function is chosen as shown in Equation (12):

$$V = \frac{1}{2}s^2 \tag{12}$$

According to the Lyapunov stability theorem, it is sufficient to prove that V < 0, in which case the system is asymptotically stable. Equation (13) can be derived from Equations (10) and (12).

$$\dot{V} = -\varepsilon|x_1|\mathrm{sgn}(s)s - ks^2 \tag{13}$$

where ε > 0, k > 0, and sgn(s)s > 0: It follows that V < 0. Therefore, the system error can converge to 0 in a finite time, making the system stable. Meanwhile, the saturation function sat(s, δ) is used instead of sgn(s), which can effectively suppress the jitter and further improve the robustness of the system. The saturation function sat(s, δ) is selected as shown in Equation (14).

$$\mathrm{sat}(s,\delta) = \begin{cases} 1 & s > \delta \\ \dfrac{s}{\delta} & |s| < \delta \\ -1 & s < -\delta \end{cases} \tag{14}$$

Design of the Expansion Observer

The control law designed using the sliding mode surface accounts for motor parameter variations and load torque perturbations. Since the perturbation value cannot be measured, this paper designs a perturbation observer for estimation. In the actual motor speed control system, the system parameter perturbations change slowly, and the first-order derivative of the perturbation can be approximated as zero.

The system state-space equation is given by Equation (15).

$$\begin{cases} \dot{\omega}_m = \dfrac{3p\psi_f}{2J}i_q - \dfrac{B}{J}\omega_m + \beta \\ \dot{\beta} = 0 \\ y = \omega_m \end{cases} \tag{15}$$

Taking ω_m and β as the observation objects to establish the gain feedback for the speed estimation error e_1, the extended disturbance observer is designed based on Equation (15), as shown in Equation (16).

$$\begin{cases} \dot{\hat{\omega}}_m = \dfrac{3p\psi_f}{2J} i_q - \dfrac{B}{J}\hat{\omega}_m + \hat{\beta} + \dfrac{\lambda_1}{\eta} e_1 \\ \dot{\hat{\beta}} = \dfrac{\lambda_2}{\eta^2} e_1 \\ e_1 = \omega_m - \hat{\omega}_m \end{cases} \tag{16}$$

where: $\hat{\omega}_m$ and $\hat{\beta}$ are the electrical angular velocity estimation, and load parameter uptake estimation, respectively; λ_1, λ_2, and η are positive real numbers. To achieve high gain, η is set to a small value. Using this observer allows not only the estimation of the disturbance terms $\hat{\beta}$ related to motor parameter variations and load torque, which can be used for feedforward compensation in the sliding mode control, but also ensures that $\hat{\beta}$ converges to β and $\hat{\omega}_m$ converges to ω_m.

From Equations (15) and (16), the error equation of the extended observer is given by Equation (17).

$$\begin{cases} \dot{e}_1 = \left(\dfrac{\lambda_1}{\eta} - \dfrac{B}{J}\right) e_1 + e_2 \\ \dot{e}_2 = \dfrac{\lambda_2}{\eta^2} e_1 \end{cases} \tag{17}$$

where e_1 denotes the speed estimation error; e_2 denotes the system parameters, and load torque estimation error.

The error equation of the state for the extended observer is shown in Equation (18).

$$\dot{e} = Ae + B\beta \tag{18}$$

where $A = \begin{bmatrix} \dfrac{\lambda_1}{\eta} - \dfrac{B}{J} & 1 \\ \dfrac{\lambda_2}{\eta} & 0 \end{bmatrix}$; $B = \begin{bmatrix} 0 \\ 1 \end{bmatrix}$; $e = \begin{bmatrix} e_1 \\ e_2 \end{bmatrix}$.

Substituting the observed perturbations and load torque uptake values into Equation (11), Equation (19) is obtained.

$$i_q^* = \frac{1}{D}\int c\dot{x}_1 + \frac{B}{J}\dot{\hat{\omega}}_m + \varepsilon|x_1|sat(s) + ks - \dot{\hat{\beta}}dt \tag{19}$$

From equation (19), it can be seen that parameter variations and load perturbations are used for feed-forward compensation. When both the load and motor parameters change, the controller can mitigate the effects of these perturbations on the system, thereby effectively improving system stability.

Experimental Methods

Simulation Experiments of the Control System

The simulation environment for the control system consists of 256GB of RAM, a 64-bit Windows 10 operating system, and MATLAB 2021b/Simulink as the simulation software. To verify the feasibility of the ISMDO-SMC algorithm proposed in this paper, simulation experiments were conducted on the control system. The control test groups include the Proportional-Integral-Derivative (PID) algorithm, the classical Sliding Mode Control (SMC) algorithm, and the Optimized Sliding Mode Control (OSMC) algorithm. The simulation setup of the control system is shown in figure 6.

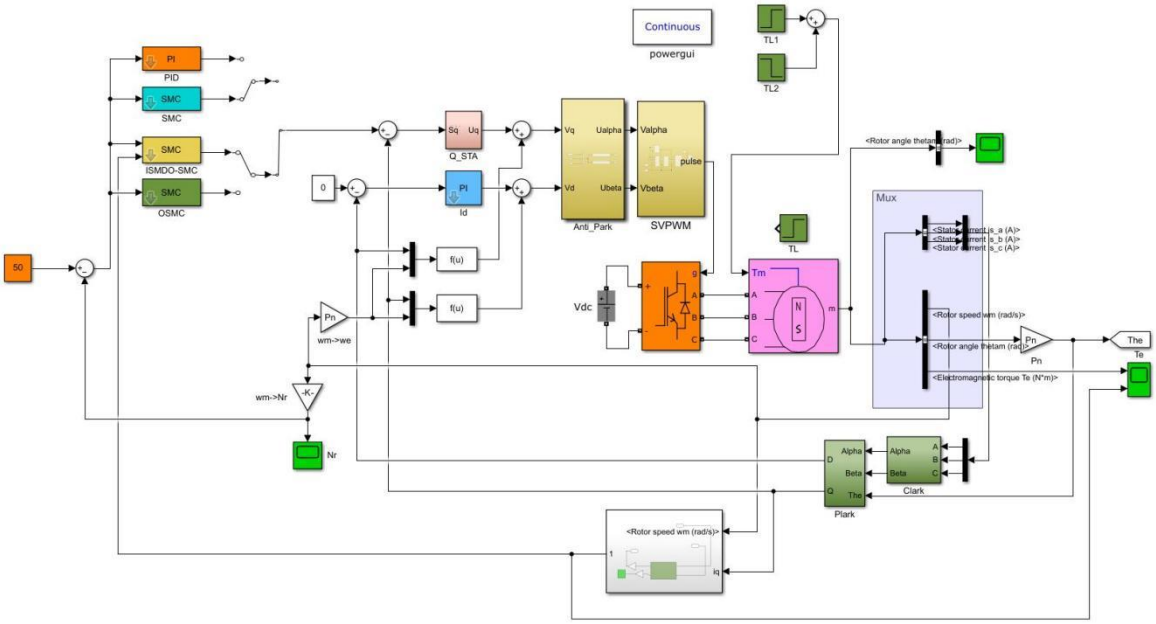

Fig. 6 - Simulation experiment of the control system

Bench Experiment

To investigate the fertilization precision of the control system, an experiment was conducted using a self-designed experimental setup, as shown in figure 7. The experimental material was "*Siyu* 335" corn seed, which was manually screened to ensure the purity of the seeds reached 100%. The moisture content of the corn seeds was (11.4 ± 0.2) %, and the mass of 1,000 kernels was (323.0 ± 0.3) g. The fertilizer used in this experiment was sulfur-containing, potassium-controlled slow-release urea. The experimental setup is based on the principle of relative motion, using the relative movement of the seed bed belt in relation to the device, thereby simulating the forward operation of the machine. Parameters such as the amount of fertilizer dispensed, the speed of the fertilizer discharge motor, and the hole spacing are controlled through the system. The fertilizer discharger opening was set to 10 mm, with rotational speeds of the fertilizer discharger at 30, 40, and 50 r/min. Four control strategies were tested in the experiment. The amount of fertilizer applied and the coefficient of variation of the grooved wheel's rotation over one week were used as performance indexes to assess the impact of fertilizer application and variation on the stability of the control system.

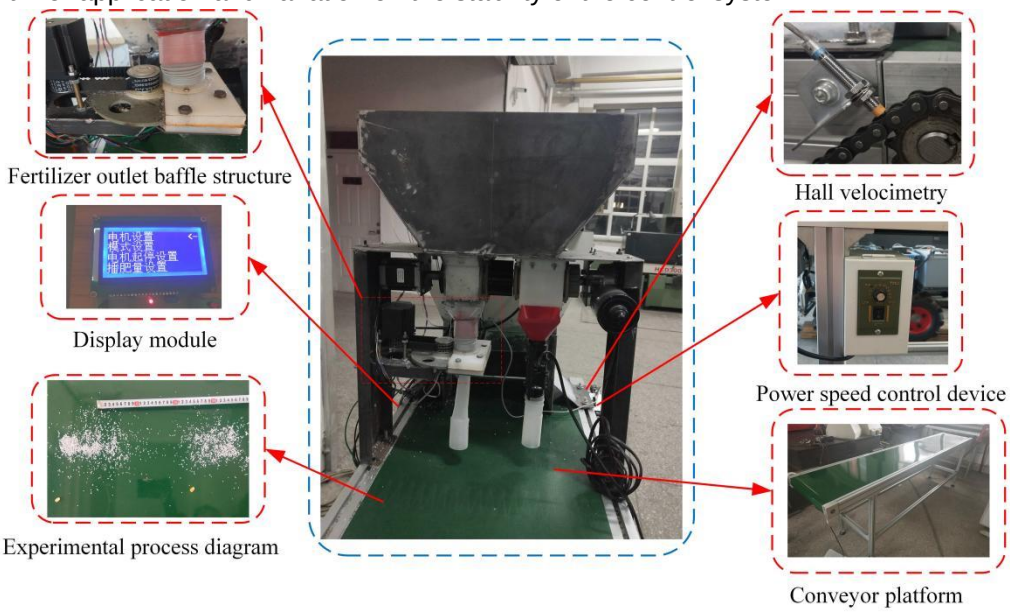

Fig. 7 - Self-designed experimental bench

The fertilizer discharger opening, fertilizer discharge shaft speed, and forward speed are key factors affecting the effectiveness of fertilizer application. These parameters interact with and constrain each other.

The difference between the sum of the actual fertilizer application rates and the theoretical fertilizer application rate in the stationary state for each group represents the fertilizer application error. A multifactor experiment was conducted, with the fertilizer application error and seed-fertilizer spacing error as performance indexes, to investigate their effects on the stability of the system under different operating parameters. The factor codes are shown in Table 1.

Table 1

Factor codes

Coded value	Factor		
	Forward speed x_1 (km/h)	Fertilizer discharge shaft speed x_2 (r/min)	Fertilizer discharger opening x_3 (mm)
1.682	3.6	50	25
1	3.28	45.9	20.9
0	2.8	40	15
-1	2.32	34.1	9.1
-1.682	2.0	30	5

RESULTS AND DISCUSSIONS

Stepper Motor Simulation Results Analysis

The target speed was set to 50 r/min, the DC side voltage to 311 V, and the initial load to 1 Nm. Figure 8 shows the speed response curves of the ISMDO-SMC, OSMC, PID, and SMC algorithms when a load of 10 Nm is abruptly applied at 0.75 s.

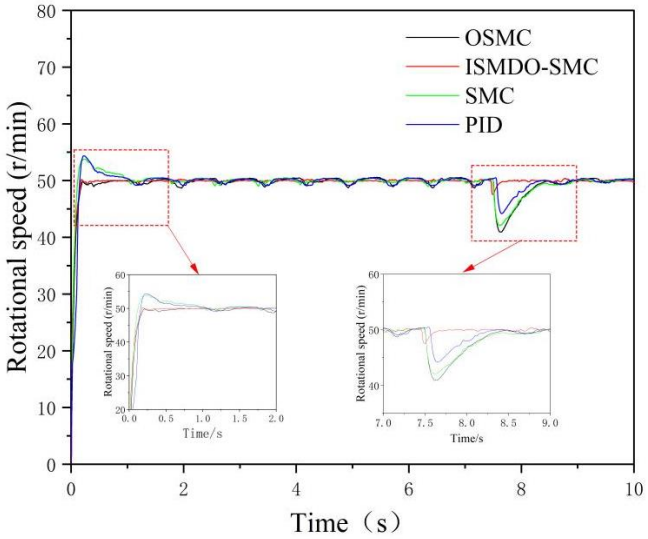

Fig. 8 - Speed response curves of the PID, SMC, ISMDO-SMC, and OSMC algorithms

From Figure 8, it can be observed that, during the starting phase, there are significant differences in the response time and the ability to follow the setpoint quickly across the four algorithms. The fast response and initial stability of the algorithms during startup affect the time required to reach the target speed. Large overshoot and oscillations typically occurred during the PID control startup phase, indicating that PID control produced significant fluctuations initially, which may cause the system to take a longer time to stabilize. The SMC algorithm performed slightly better than PID control, though some overshoot still occurred. The OSMC exhibited smoother performance at startup and was able to approach the target speed quickly with fewer fluctuations. The ISMDO-SMC showed almost no overshoot at the beginning and reached the set speed rapidly, demonstrating excellent control. After the sudden load addition, the PID, SMC, and OSMC all showed significant fluctuations and took a long time to return to a steady state. Among them, OSMC had the largest fluctuations and took the longest time to recover. In contrast, the ISMDO-SMC performed the best under sudden load changes, quickly suppressing the disturbances. In summary, the ISMDO-SMC reached the target speed faster and more smoothly during startup and exhibited superior resistance to disturbances with fast recovery after a sudden load change. In this study, the dynamic and anti-interference performance of four control algorithms (PID, SMC, ISMDO-SMC, and OSMC) were quantitatively analyzed and compared, as shown in Table 2.

The PID and SMC algorithms exhibited varying degrees of overshoot, 9% and 7.4%, respectively, and longer regulation times, 1.12 s and 1.03 s, respectively. The OSMC required 0.35 s more to regulate than the ISMDO-SMC algorithm, although it showed no overshoot. In terms of anti-jamming performance, the ISMDO-SMC algorithm demonstrated the best capability, with a descending speed of only 2.5 r/min and the shortest recovery time to steady state of 0.13 s. The OSMC algorithm had the longest recovery time of 0.85 s, with a descending speed of 9 r/min. In comparison, the PID and SMC algorithms had steady-state restoration times of 0.73 s and 0.75 s, respectively. The OSMC's performance was weaker, with a longer recovery time and higher descending speed. Overall, the ISMDO-SMC algorithm showed significant advantages in both dynamic and anti-interference performance. It achieved zero overshoot, with a peak time of 0.18 s and a regulation time of 0.42 s, both of which were significantly better than those of the other algorithms.

Table 2

Comparison of dynamic performance and anti-interference performance of PID, SMC, ISMDO-SMC, and OSMC algorithms

Algorithm	Overshoot	Peak time (t/s)	Regulation time (t/s)	Down speed (r/min)	Recovery of steady state time (t/s)
PID	9%	0.22	1.12	6	0.73
SMC	7.4%	0.25	1.03	8	0.75
ISMDO-SMC	0	0.18	0.42	2.5	0.13
OSMC	0	0.2	0.77	9	0.85

To verify that the designed expanding sliding mode observer exhibited good robustness to the system, the ISMDO-SMC algorithm was used to apply a torque of 10 Nm abruptly at 7.5 s and to unload the torque at 10.5 s. Figure 9 shows the comparison between the estimated and actual torque during sudden load addition and removal by the expanding observer. The actual torque curve in the steady-state phase showed jitter between 0 and 7.5 s, and between 10.5 s and 15 s, with an average magnitude of approximately ±0.2 Nm. This jitter may have been caused by sensor noise or mechanical disturbances inside the motor. The estimated torque exhibited a significant step change near 7.5 s and 10.5 s, followed by a rise in the actual torque response, though with noticeable delays and overshoots. The peak value of the actual torque reached 1.1 times the set value at 7.5 s, corresponding to an overshoot of about 10%. This overshoot suggests that the control gain may have been set too high, leading to an over-response to the target torque. To reduce this overshoot, it may be necessary to lower the gain or mitigate the overshoot by introducing a derivative term. During sudden torque changes, the ISMDO-SMC algorithm provided a smoother torque estimation than the actual measured torque. Therefore, the perturbed values of estimated motor parameter variations and load torque, recorded by the expanding observer, can be effectively used in the sliding mode controller.

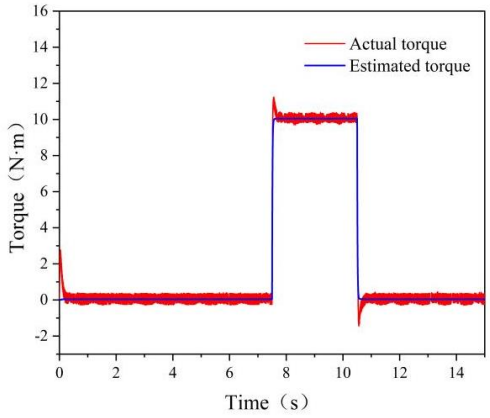

Fig. 9 - Comparison between the estimated and actual torque during sudden load addition and removal by the expanding observer

Fertilizer precision experiment

Figure 10 shows the distribution of fertilizer application amounts for the control algorithms (PID, SMC, ISMDO-SMC, and OSMC) at rotational speeds of 30, 40, and 50 r/min.

From the dynamic characteristics of the fertilizer application distribution, significant differences in stability performance were observed across the four control algorithms at different rotational speeds. The PID

algorithm exhibited large fluctuations in the amount of fertilizer applied, particularly at high rotational speeds (50 r/min), where both the fluctuation amplitude and extreme values increased significantly, indicating poor stability. The SMC algorithm improved the fluctuation amplitude compared to PID, resulting in a smoother distribution of the fertilizer application amount. However, it was still unable to completely eliminate the impact of large disturbances under complex working conditions. The OSMC algorithm significantly reduced the fluctuation amplitude by optimizing the sliding mode control, especially at high rotational speeds, where the distribution became more concentrated, demonstrating strong anti-disturbance capabilities. The ISMDO-SMC algorithm exhibited the smallest fluctuation amplitude and the smoothest distribution of fertilizer application at all rotational speeds. Even at the high speed of 50 r/min, the amount of fertilizer applied remained stable. Overall, the fertilization stability of the four control algorithms is ranked as follows: ISMDO-SMC > OSMC > SMC > PID. The ISMDO-SMC control algorithm significantly outperforms the others and is well-suited for scenarios that require high fertilization stability under complex working conditions.

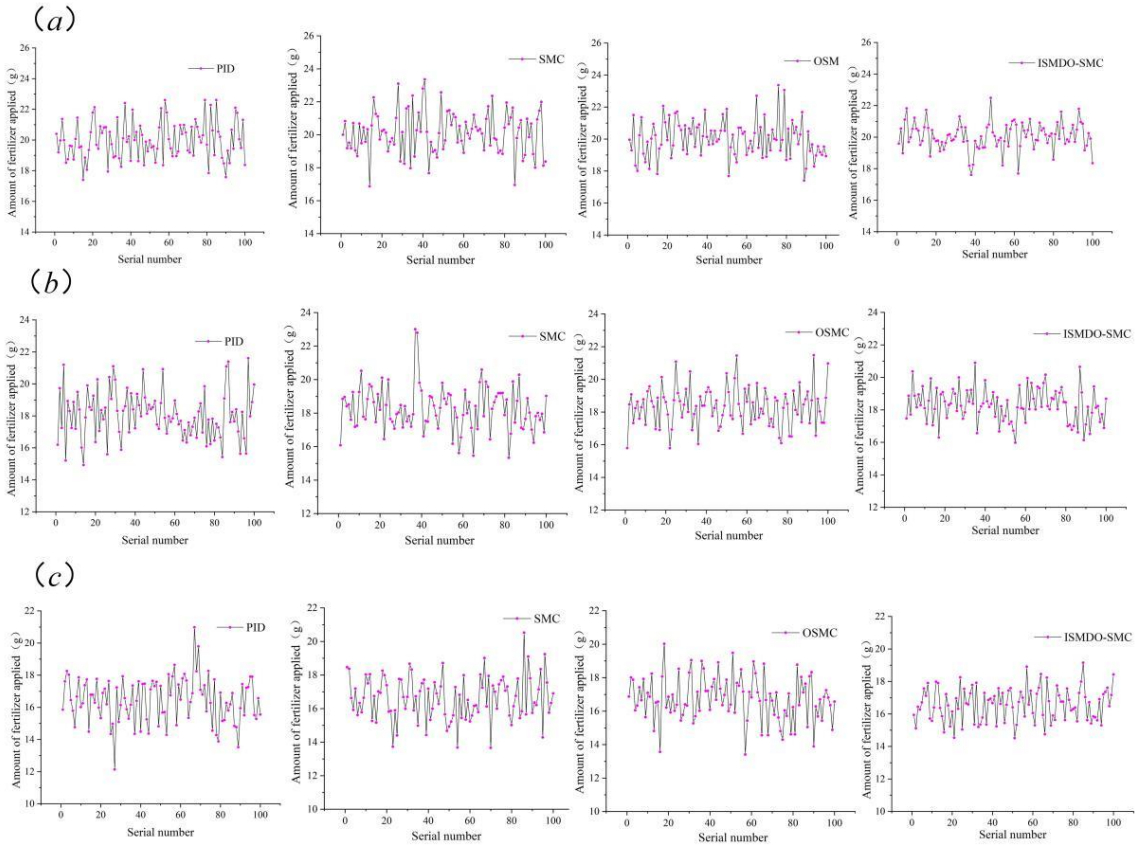

Fig. 10 - Distribution of fertilizer application amounts for the control algorithms (PID, SMC, ISMDO-SMC, and OSMC). (a) 30 r/min; (b) 40 r/min; (c) 50 r/min

Figure 11 shows the distribution of the coefficient of variation for the four control algorithms (PID, SMC, ISMDO-SMC, and OSMC) at rotational speeds of 30, 40, and 50 r/min. The coefficient of variation for the PID algorithm increased progressively with speed, from 6.50% at 30 r/min to 8.60% at 50 r/min, indicating poor performance in handling dynamic disturbances at high rotational speeds and a significant decrease in the stability of the fertilizer application system. The SMC algorithm partially compensated for the perturbations using sliding mode control, with coefficients of variation of 6.10%, 7.20%, and 8.20% at 30, 40, and 50 r/min, respectively. While this showed improvement over PID control, it did not completely resolve the issue of large fluctuations at high speeds. The OSMC algorithm further optimized sliding mode control, achieving coefficients of variation of 5.70%, 6.30%, and 7.60%, which were significantly lower than those of PID and SMC, demonstrating better robustness and anti-disturbance capability. The ISMDO-SMC algorithm exhibited the lowest coefficients of variation, at 4.90%, 5.70%, and 6.50%, respectively, and demonstrated the best stability across all rotational speeds. The dynamic disturbance suppression capability of the system was further enhanced by the intelligent optimization algorithm, effectively controlling fluctuations in the fertilizer application system. Therefore, based on the coefficient of variation, the stability of the four control algorithms is ranked as follows: ISMDO-SMC > OSMC > SMC > PID. The ISMDO-SMC algorithm significantly reduced the variability in fertilizer application, making it particularly suitable for scenarios that require high accuracy and stability in fertilizer application.

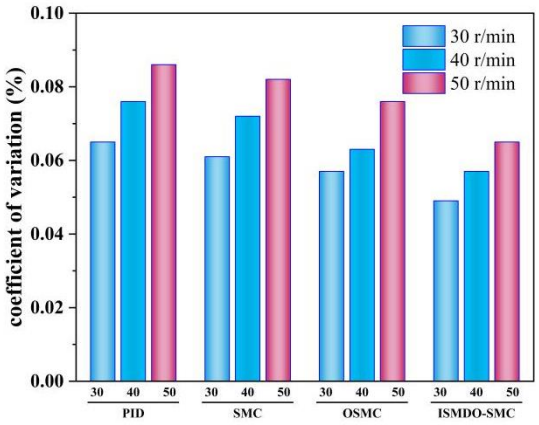

Fig. 11. Distribution of the coefficient of variation for the four control algorithms (PID, SMC, ISMDO-SMC, and OSMC)

Multi-factor Parameter Optimization Analysis

The experimental scheme and results are shown in Table 3. The regression equations for the factors influencing fertilizer application error and seed-fertilizer spacing error were obtained through multiple regression fitting using Design-Expert 8.0.6 software. The results of the analysis of variance (ANOVA) for the regression equations are shown in Table 4. The regression equations for both groups were highly significant ($P < 0.01$). The misfit P-value was not significant, indicating a good fit for the equation. The ANOVA results for fertilizer application error showed a P-value of 0.55 for the misfit term, indicating that no other factors affected the fertilizer application error. The ANOVA results for seed-fertilizer spacing error showed a misfit P-value of 0.06, indicating that no other factors influenced seed-fertilizer spacing error. After confirming that the models were significant and the misfit terms were not significant, the insignificant factors were removed, and the factor-coded regression equations (20-21) were developed.

$$y_1 = 140.92 - 4.03x_2 + 4.71x_3 + 15.23x_1^2 + 0.02x_2^2 \quad (20)$$

$$y_2 = 41.04 - 16.55x_1 - 0.69x_3 + 0.21x_1x_2 \quad (21)$$

where y_1 is the fertilizer application error, g; y_2 is the seed-fertilizer spacing error, mm; x_1 is the forward speed, km/h; x_2 is the fertilizer discharge shaft speed, r/min; and x_3 is the fertilizer discharger opening, mm.

Table 3

Experimental scheme and results

Experiment number	Forward speed x_1 (km/h)	Fertilizer discharge shaft speed x_2 (r/min)	Fertilizer discharger opening x_3 (mm)	Fertilizer application error y_1 (g)	Seed-fertilizer spacing error y_2 (mm)
1	1	1	1	3.46	4.6
2	1	1	-1	4.02	3.48
3	1	-1	1	18.67	2.76
4	1	-1	-1	6.32	2.16
5	-1	1	1	8.91	3
6	-1	1	-1	2.9	2.76
7	-1	-1	1	15.35	2.4
8	-1	-1	-1	4.25	3.6
9	-1.682	0	0	15.33	3.24
10	1.682	0	0	12.01	4.8
11	0	-1.682	0	19.87	3
12	0	1.682	0	3.89	3.36
13	0	0	-1.682	3.47	1.8
14	0	0	1.682	6	4.2
15	0	0	0	1.38	2.64
16	0	0	0	1.87	3.6
17	0	0	0	2.35	3.48
18	0	0	0	1.92	2.88
19	0	0	0	2.07	3.6
20	0	0	0	8.46	3.36
21	0	0	0	2.23	2.88
22	0	0	0	10.92	3.12
23	0	0	0	2.11	3.24

The experiment on the coefficients of the regression equations showed that the effects of the forward speed, fertilizer discharger opening, and fertilizer discharge shaft speed on fertilizer application error increased gradually. Fertilizer application error is an important indicator for assessing the performance of the fertilization system. Therefore, this paper focuses on analyzing the effects of interactions among various factors on fertilizer application error. To intuitively analyze the relationship between the test factors and fertilizer application error, Design-Expert 6.0.8 software was used to generate the response surface diagrams of the forward speed, fertilizer discharger opening, and fertilizer discharge shaft speed on the fertilizer application error indexes, as shown in figures 12-14.

Table 4

Results of the analysis of variance for the regression equations

Source of variance	Fertilizer application error (g)				Seed-fertilizer spacing error (mm)			
	Square sum	Degrees of freedom	*F*	*P*	Square sum	Degrees of freedom	*F*	*P*
Model	585.75	9	5.77	0.002**	7.99	9	4.00	0.012*
x_1	1.95	1	0.17	0.685	1.19	1	5.35	0.038*
x_2	204.92	1	18.16	0.001**	0.83	1	3.73	0.076
x_3	72.08	1	6.39	0.025*	1.93	1	8.70	0.011*
x_1x_2	11.81	1	1.05	0.325	1.44	1	6.50	0.024*
x_1x_3	3.54	1	0.31	0.585	0.90	1	4.04	0.066
x_2x_3	40.50	1	3.59	0.081	0.48	1	2.16	0.165
x_{12}	166.95	1	14.80	0.002**	0.89	1	3.99	0.067
x_{22}	111.27	1	9.86	0.008**	0.03	1	0.13	0.721
x_{32}	1.16	1	0.10	0.753	0.17	1	0.76	0.399
Residual	146.66	13			2.89	13		
Lost proposal	50.80	5	0.85	0.553	1.94	5	3.26	0.067
Errors	95.85	8			0.95	8		
Sum of all	732.41	22			10.88	22		

Note: * indicates significant (P < 0.05) and ** indicates highly significant (P < 0.01).

Figure 12 shows the effect of the interaction between x_1 and x_2 on the fertilizer application error when x_3 is 15 cm. When x_1 is certain, with the increase of x_2, the error in the amount of fertilizer applied firstly decreases and then increases by a small margin. When x_2 is certain, the error in the amount of fertilizer applied decreases first and then increases with the increase of x_1. However, in terms of magnitude, the magnitude of the fertilizer application error size influenced by the rotational speed exceeds the influence of the forward speed, so the appropriate speed of the fertilizer discharger can reduce the error.

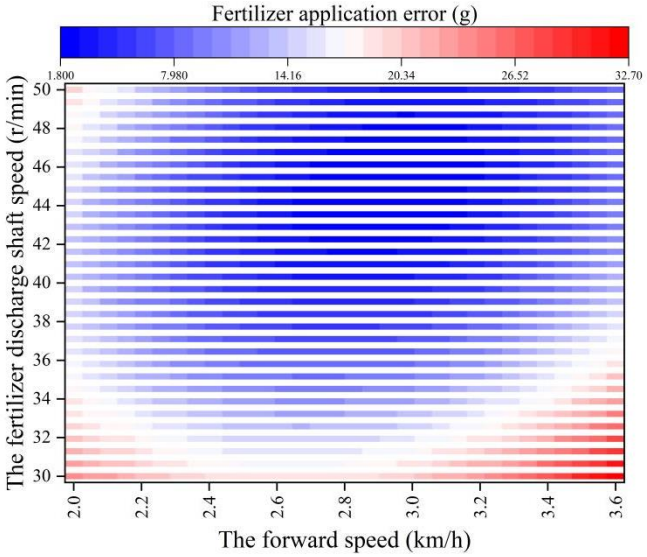

Fig. 12 - Interaction between forward speed and fertilizer discharge shaft speed on the fertilizer application error

Figure13 shows the effect of the interaction between x_1 and x_3 on fertilizer application error when x_2 is 40 r/min. At a fixed forward speed, the fertilizer application error gradually increases with the increase of x_3. When x_3 is fixed, the fertilizer application error first decreases and then increases as forward speed increases. Therefore, selecting a smaller fertilizer discharger opening and driving at a moderate speed can effectively reduce the fertilizer application error.

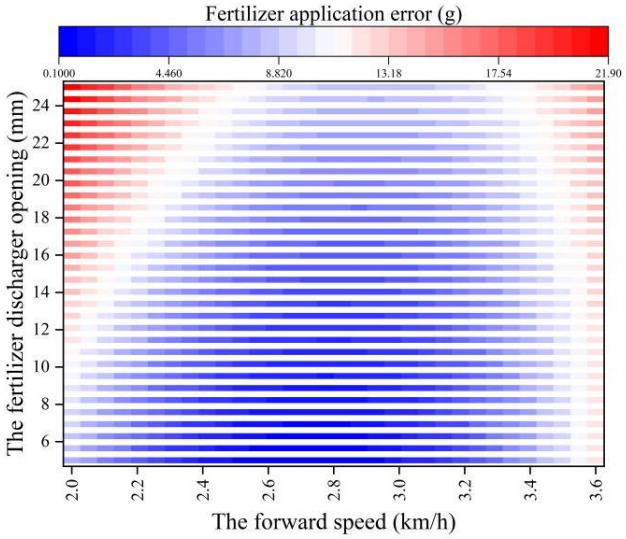

Fig. 13 - Interaction between forward speed and fertilizer discharger opening on the fertilizer application error

Figure 14 shows the effect of the interaction between x_2 and x_3 on fertilizer application error when x_1 is 2.8 km/h. When x_3 is larger, the fertilizer application error with x_2 gradually decreases, with a noticeable amplitude. When x_3 is smaller, the fertilizer application error first decreases and then increases with x_2, with a smaller and less noticeable magnitude. When x_2 is fixed, the overall fertilizer application error increases gradually as x_3 increases.

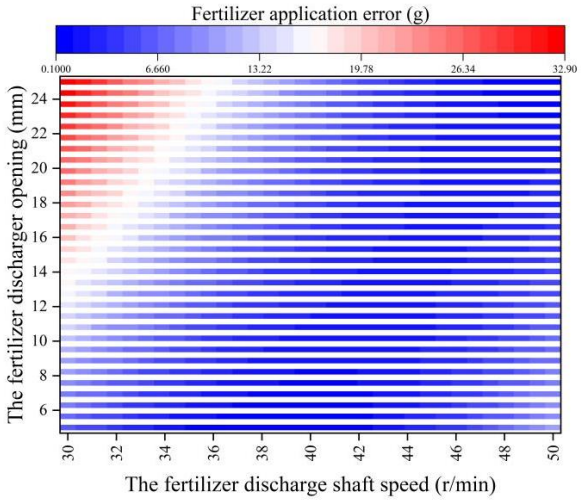

Fig. 14 - Interaction of fertilizer discharge shaft speed and fertilizer discharger opening on the fertilizer application error

Optimizing the best combination of parameters using the software requires setting the boundary conditions, and the mathematical model was developed as shown in equation (22).

$$\begin{cases} min\, y_1 \\ min\, y_2 \\ s.t. \begin{cases} 2\,km/h \le x_1 \le 3.6\,km/h \\ 30\,r/min \le x_2 \le 50r/min \\ 5\,mm \le x_3 \le 25mm \end{cases} \end{cases} \quad (22)$$

The optimization module in Design-Expert 8.0.6 software completed the parameter optimization. When the forward speed was 2.8 km/h, the fertilizer discharge shaft speed was 42 r/min, and the fertilizer discharger opening was 5.5 mm, the fertilizer application error and seed-fertilizer spacing error were minimized. Three sets of repetitive tests were conducted based on the optimized parameters, and the results showed that the error between the actual and optimized fertilizer application amounts was about 0.32, while the seed-fertilizer spacing error was 0.21. These results indicate that the optimized parameters effectively completed the fertilizer application operation. Under the condition of the optimal parameter combination, the fertilizer application error and seed-fertilizer spacing error in actual operation were 1.7 g and 2.2 mm, respectively.

CONCLUSIONS

(1) A control system for synchronizing corn seeding and precision hole fertilization was designed. The sliding mode controller with integral variable structure utilizes observed changes in motor parameters as feed-forward compensation, enabling the speed control system to respond quickly without overshoot. The jitter is minimal, and the regulation time is short under sudden load addition or removal, effectively suppressing the oscillations typically associated with sliding mode control.

(2) The mathematical model of the motor was established, and the controller was designed and simulated. The simulation results showed that the ISMDO-SMC algorithm had 0% overshoot, a peak time of 0.012 seconds, a regulation time of only 0.02 seconds, a steady-state recovery time of 0.02 seconds, and a descending rotational speed of 4 r/min, indicating the strongest dynamic response and stability. Additionally, the ISMDO-SMC algorithm demonstrated the lowest coefficient of variation for fertilizer application compared to the PID, SMC, and OSMC algorithms, with coefficients of variation of 4.90%, 5.70%, and 6.50% for rotational speeds of 30, 40, and 50 r/min, respectively.

(3) The regression equations of each factor on fertilizer application error and seed-fertilizer spacing error were obtained by fitting the experimental data with multiple regression. The mathematical model for parameter optimization was established through multi-objective variable optimization, yielding the optimal parameter combination. The optimal parameters were determined to be 1.7 g for fertilizer application error and 2.2 mm for seed-fertilizer spacing error, with the forward speed of 2.8 km/h, the fertilizer discharge shaft speed of 42 r/min, and the fertilizer discharger opening of 5.5 mm. These results demonstrate that the control system can significantly improve the stability and precision of fertilizer application and seeding, providing valuable insights for the development of fertilizer application control systems.

ACKNOWLEDGEMENT

This research was funded by the China Postdoctoral Science Foundation, grant number 2024MD763975; the School Orientation Training Research Initiation Fund Program, grant number XYB202307; the Heilongjiang Provincial Postdoctoral General Funding Project, grant number LBH-Z24250; the National Key Research and Development Program, grant number 2016YFD0200600.

REFERENCES

[1] Alameen, A., Al-Gaadi, K., & Tola, E. (2019). Development and performance evaluation of a control system for variable rate granular fertilizer application. Computers and Electronics in Agriculture, *160*, 31-39. https://doi:10.1016/j.compag.2019.03.011

[2] Bu, H., Yu, S., Dong, W., Zhang, L., & Xia, Y. (2022). Analysis of the Effect of Bivariate Fertilizer Discharger Control Sequence on Fertilizer Discharge Performance. *Agriculture*, *12*(11), 1927. https://doi:10.3390/agriculture12111927

[3] Chen, H., Zheng, J., Lu, S., Zeng, S., & Wei, S. (2021). Design and experiment of vertical pneumatic fertilization system with spiral Geneva mechanism. *International Journal of Agricultural and Biological Engineering*, *14*(3), 135-144. https://doi:10.25165/j.ijabe.20211404.6575

[4] Cheng, B., He, R., Xu, Y., & Zhang, X. (2022). Simulation Analysis and Test of Pneumatic Distribution Fertilizer Discharge System. *Agronomy*, *12*(10), 2282. https://doi:10.3390/agronomy12102282

[5] Du, S., Wang, S., Wang, Y., Jia, L., Sun, W., & Liu, Y. (2023). Design of Sensorless Control System for Permanent Magnet Linear Synchronous Motor Based on Parametric Optimization Super-Twisting Sliding Mode Observer. *Electronics*, *12*(12), 2553. https://doi:10.3390/electronics12122553

[6] Pramod P., Madhukar Nalawade, S., Balasaheb Bhanage, G., Ashok Walunj, A., Bhaskar Kadam, P., G Durgude, A., & R Patil, M. (2023). Variable rate fertilizer application technology for nutrient management: A review. *International Journal of Agricultural and Biological Engineering*, *16*(4), 11-19. https://doi:10.25165/j.ijabe.20231604.7671

[7] Qi, Z., Liu, C., Wang, Y., Zhang, Z., & Sun, X. (2024). Design and Experimentation of Targeted Deep Fertilization Device for Corn Cultivation. *Agriculture*, *14*(9), 1645. https://doi:10.3390/agriculture14091645

[8] Shi, Y., Hu, Z., Wang, X., Odhiambo, M., & Ding, W. (2018). Motion analysis and system response of fertilizer feed apparatus for paddy Variable-Rate fertilizer spreader. *Computers and Electronics in Agriculture*, *153*, 239-247. https://doi:10.1016/j.compag.2018.08.021

[9] Sugirbay, A. M., Zhao, J., Nukeshev, S. O., & Chen, J. (2020). Determination of pin-roller parameters and evaluation of the uniformity of granular fertilizer application metering devices in precision farming. *Computers and Electronics in Agriculture*, *179*, 105835. https://doi:10.1016/j.compag.2020.105835

[10] Tola, E., Kataoka, T., Burce, M., Okamoto, H., & Hata, S. (2008). Granular fertiliser application rate control system with integrated output volume measurement. *Biosystems Engineering*, *101*(4), 411-416. https://doi:10.1016/j.biosystemseng.2008.09.019

[11] Vieira-Megda, M. X., Mariano, E., Leite, J. M., Franco, H. C. J., Vitti, A. C., Megda, M. M., Khan, S.A., Mulvaney, R.L., & Trivelin, P. C. O. (2015). Contribution of fertilizer nitrogen to the total nitrogen extracted by sugarcane under Brazilian field conditions. *Nutrient Cycling in Agroecosystems*, *101*(2), 241-257. https://doi:10.1007/s10705-015-9676-7

[12] Wang, J., Wang, Z., Weng, W., Liu, Y., Fu, Z., & Wang, J. (2022). Development status and trends in side-deep fertilization of rice. *Renewable Agriculture and Food Systems*, *37*(5), 550-575. https://doi:10.1017/s1742170522000151

[13] Wang, Y., Tan, Y., Wei, S., Liao, M., Zang, Y., & Zeng, S. (2023). Design and experimental study of the fertilizer applicator with vertical spiral fluted rollers. *International Journal of Agricultural and Biological Engineering*, *16*(5), 80-87. https://doi:10.25165/j.ijabe.20231605.7555

[14] Yu, C., Wang, Q., Cao, X., Wang, X., Jiang, S., & Gong, S. (2021). Development and Performance Evaluation of a Precise Application System for Liquid Starter Fertilizer while Sowing Maize. *Actuators*, *10*(9), 221. https://doi:10.3390/act10090221

[15] Yu, H., Ding, Y., Fu, X., Liu, H., Jin, M., Yang, C., Liu, Z., Sun, G., & Dou, X. (2019). A solid fertilizer and seed application rate measuring system for a seed-fertilizer drill machine. *Computers and Electronics in Agriculture*, *162*, 836-844. https://doi:10.1016/j.compag.2019.05.007

[16] Zhang, R., Zhao, C., Wang, X., Meng, Z., Chen, L., & Ma, W. (2012). A Variable-Rate Fertilizer Control System for Disc Fertilizer Spreaders. *Intelligent Automation & Soft Computing*, *18*(5), 461-467. https://doi:10.1080/10798587.2012.10643256